This document is downloaded from DR-NTU (https://dr.ntu.edu.sg)
Nanyang Technological University, Singapore.

Improved stability of Y2O3 supported Ni catalysts for CO2 methanation by precursor-determined metal-support interaction

Yan, Yong; Dai, Yihu; Yang, Yanhui; Lapkin, Alexei A.

2018

Yan, Y., Dai, Y., Yang, Y., & Lapkin, A. A. (2018). Improved stability of Y2O3 supported Ni catalysts for CO2 methanation by precursor-determined metal-support interaction. Applied Catalysis B: Environmental, 237, 504-512. doi:10.1016/j.apcatb.2018.06.021

https://hdl.handle.net/10356/138847

https://doi.org/10.1016/j.apcatb.2018.06.021

© 2018 Elsevier B.V. All rights reserved. This paper was published in Applied Catalysis B: Environmental and is made available with permission of Elsevier B.V.

Downloaded on 27 Aug 2022 14:49:01 SGT

Applied Catalysis B: Environmental xxx (2018) xxx-xxx

Contents lists available at ScienceDirect

Applied Catalysis B: Environmental

journal homepage: www.elsevier.com

Improved stability of Y_2O_3 supported Ni catalysts for CO_2 methanation by precursor-determined metal-support interaction

Yong Yan[a, b, *], Yihu Dai[a, c, **], Yanhui Yang[a, c], Alexei A. Lapkin[a, d]

[a]Cambridge Centre for Advanced Research and Education in Singapore Ltd., 1 Create Way, CREATE Tower #05-05, Singapore, 138602, Singapore
[b]School of Chemical and Biomedical Engineering, Nanyang Technological University, Singapore, 637459, Singapore
[c]Institute of Advanced Synthesis, School of Chemistry and Molecular Engineering, Jiangsu National Synergetic Innovation Center for Advanced Materials, Nanjing Tech University, Nanjing, 211816, China
[d]Department of Chemical Engineering and Biotechnology, University of Cambridge, Philippa Fawcett Drive, Cambridge, CB3 0AS, United Kingdom

ARTICLE INFO

Keywords:
Ni/Y_2O_3
Metal-Support interaction
Support precursor
CO_2methanation
Stability

ABSTRACT

Y_2O_3 supported Ni catalysts were prepared from different Y precursors. The catalysts synthesized *via* $Y_4O(OH)_9(NO_3)$ and $YO(NO_3)$ as precursors exhibit superior activity in CO_2 methanation reaction compared to the catalysts prepared by direct impregnation of Y_2O_3. $YO(NO_3)$ acts as a unique matrix to afford anchoring sites to interact with Ni^{2+} ions, leading to a moderate interaction between Ni metal and Y_2O_3 support, which translates into excellent catalytic activity and stability towards CO poisoning. *In situ* DRIFTS spectra confirm the reaction mechanism of Ni/Y_2O_3 catalyzed CO_2 methanation with carbonates and formates as the key intermediates. The apparent difference in the rate of transformation of formates into methane determines catalytic activity of these Ni/Y_2O_3 catalysts. This work provides an effective strategy to achieve CO_2 activation and resistance to CO poisoning through careful selection of precursor for the support, which allows to control the strength of metal-support interaction.

1. Introduction

Atmospheric CO_2 concentration reached 400.5 ppm in 2016, contributing 77% to the total increase in radiative forcing caused by all long-life greenhouse gases during the past 30 years [1]. Understanding consequences of the increased atmospheric CO_2 concentration stimulates the drive towards reduction in CO_2 emissions as well as the development of methods of direct use of CO_2 as a feedstock to reduce both, future use of non-renewable feedstocks, and emissions from such processes. With the developments in photocatalytic water splitting and rapid adoption of renewable electricity generation, large-scale production of H_2 at low cost is expected to be realized in the near future [2]. Thus, the reactions of direct hydrogenation of CO_2, which have been extensively studied over the years [3–6], are experiencing a renewal of interest both in academic and in industrial research. Among these, methanation of CO_2 over Ni-based catalysts is attractive due to excellent performance and low catalyst cost, yielding potential access to conventional combustion fuel and energy technology with low life-cycle carbon emissions [7–11].

Although Ni-based catalysts show comparable activity for CO_2 methanation to that of noble metal-based catalysts and thus are economically favorable, their stability is not yet at the commercially viable range. The medium-to-high operating temperature for CO_2 methanation in the highly exothermic reaction puts a difficult demand on the mechanical and chemical catalyst stability [12,13]. In the presence of CO in the feed gas or as a byproduct, formation of mobile Ni carbonyl species and sintering of active sites result in a significant loss of catalytic activity [14–16]. To improve stability towards CO poisoning, one can try to increase the strength of metal-support interaction to provide more anchoring sites for the active Ni particles. Introduction of promoters and/or change of the support have been explored to tune the metal-support interaction [17–20]. However, variations in catalyst composition result in the increased complexity in analyzing the cause-and-effect relationships. It would be of interest to de-convolute the effects and to explore the individual contributions to metal-support interaction.

* Corresponding authors at: Cambridge Centre for Advanced Research and Education in Singapore Ltd., 1 Create Way, CREATE Tower #05-05, Singapore, 138602, Singapore.
** Corresponding author.
Email addresses: yanyong@ntu.edu.sg (Y. Yan); ias_yhdai@njtech.edu.cn (Y. Dai)

https://doi.org/10.1016/j.apcatb.2018.06.021
Received 13 February 2018; Received in revised form 23 May 2018; Accepted 6 June 2018
Available online xxx
0926-3373/ © 2018.

UNCORRECTED PROOF

Recently, Y_2O_3 has been introduced as a promoter in several catalytic systems [21]. Dispersion of Cu over $Cu/ZnO/Al_2O_3$ catalysts was significantly improved by introduction of a moderate amount of Y_2O_3 [22]. Similarly, addition of Y_2O_3 into Cu–SAPO-34 catalysts promoted their activity in selective reduction of NO_x by NH_3 *via* an enrichment of the stable isolated Cu species and surface acidic sites [23]. In the case of Ni/Al_2O_3, Y_2O_3 doping not only increased catalytic activity in autothermal reforming of methane with CO_2 into syngas, but also improved catalyst stability [24]. Y_2O_3 has also been directly applied as a support for Ni based catalysts, due to its distinct surface properties [25–28]. Ni/Y_2O_3 demonstrated excellent activity in CO_2 methanation, compared to Ni supported onto different metal oxides [29]. But, the CO poisoning effects and metal-support interaction in the Y_2O_3-supported Ni catalysts are not well studied.

In this work, we tune the metal-support interaction *via* choosing appropriate Y-precursors. Catalysts obtained from different Y-precursors have the same composition and pore structure, but the differences in the anchoring sites in the supports obtained from the different precursors afford different interactions with the Ni species which, in turn, determine catalytic activity and stability to CO poisoning. Through this method, we are able to study the effect of the strength of metal-support interaction on stability and activity of the Ni-based CO_2 methanation catalysts.

2. Experimental

2.1. Catalyst preparation

The support precursor $Y_4O(OH)_9(NO_3)$ (hydroxide hydrate, HN) was obtained by hydrothermal treatment of $Y(NO_3)_3$ solutions at 120 °C for 12 h with the addition of urea, which was filtered and dried at 100 °C overnight. The support precursors $YO(NO_3)$ (oxide nitrate: ON) and Y_2O_3 (oxide: OX) were synthesized by calcination of $Y_4O(OH)_9(NO_3)$ on air for 2 h at 400 and 500 °C, respectively.

Traditional impregnation method was adopted to introduce Ni species. During impregnation, the support precursor was immersed into a solution containing the required amount of $Ni(NO_3)_2$ at a constant stirring for 0.5 h. All the Ni loadings in the prepared catalysts were carefully analysed by considering weight changes of the calcined catalysts. Excess water was removed in a rotary evaporator at 80 °C. The final Ni supported on Y_2O_3 sample was obtained by calcination on air at 500 °C for 4 h. The catalysts prepared from different support precursors (HN, ON and OX) were denoted as Ni/Y_2O_3-HN, Ni/Y_2O_3-ON and Ni/Y_2O_3-OX, respectively.

2.2. Activity test

Prior to activity tests, 100 mg of catalyst was reduced *in situ* in H_2 flow of 30 mL (STP) ·min^{-1} (25 °C, 1 atm) at 500 °C for 60 min in a fixed bed quartz tube micro-reactor. Catalytic activity measurements were carried out at atmospheric pressure by passing a gaseous mixture of CO_2 (5%) and H_2 (20%) in He balance at a total flow rate of 100 mL·min^{-1} (25 °C, 1 atm), corresponding to GHSV ~ 40,000 h^{-1}. The inlet and outlet flows were analyzed by an on-line gas chromatograph (Agilent 6890) equipped with both a FID and a TCD detectors. The sampling data were collected when reaction reached steady state, typically within 60–120 min after reaching the desired reaction temperature. Since only CH_4 and CO were identified as products in the outlet gas, conversion of CO_2 and yields of CH_4 and CO were calculated by the following equations:

$$CO_2\,\text{conversion}(\%) = \frac{[CH_4]_{out}+[CO]_{out}}{[CO_2]_{in}} \times 100$$

$$CH_4\,\text{yield}(\%) = \frac{[CH_4]_{out}}{[CH_4]_{out}+[CO]_{out}+[CO_2]_{out}} \times 100$$

$$CO\,\text{yield}(\%) = \frac{[CO]_{out}}{[CH_4]_{out}+[CO]_{out}+[CO_2]_{out}} \times 100$$

2.3. Characterization

Thermogravimetric analysis (TGA) was conducted on a PerkinElmer Diamond TG/DTA equipment. Samples were heated in N_2 up to 800 °C with a ramp of 10 °C·min^{-1}.

Concentration of Ni in the prepared catalysts was analyzed by Dualview Optima 5300 DV inductive coupled plasma optical emission spectrometry (ICP-OES) system after digestion of the solid by an aqua regia solution.

N_2 adsorption-desorption isotherms were measured using a Quantachrome Autosorb-1C instrument at liquid N_2 temperature (-196 °C). Prior to N_2 physisorption, all the catalysts were outgassed at 300 °C for 5 h in vacuum. The specific surface areas were calculated using Brunauer-Emmett-Teller (BET) isotherm in the partial pressure range of 0.05-0.35. The pore volumes and average pore diameters were determined by BJH method from the desorption branches of the isotherms.

Powder X-ray Diffraction (PXRD) patterns were recorded on a Bruker Advance 8 X-ray diffractometer using a Ni filtered Cu Kα radiation (λ = 0.154 nm), operated at 40 kV and 40 mA. PXRD data were collected between 10 and 90° (2θ) with a resolution of 0.02° (2θ).

High resolution transmission electron microscopy (HR-TEM) measurements were performed using JEOL-2010 UHR high resolution transmission electron microscope with an accelerating voltage of 200 kV.

CO_2 temperature-programmed desorption (CO_2-TPD) and CO temperature-programmed desorption (CO-TPD) experiments were performed using a Micromeritics Autochem II 2920 instrument equipped with a quadrupole mass spectrometer (MKS Cirrus). Prior to TPD experiments, samples of 100 mg were pre-treated at 500 °C in H_2 for 60 min and then cooled to ambient temperature. The sample was then exposed to 20% CO_2/Ar or 5% CO/Ar for 60 min, followed by Ar purge for another 60 min. Temperature was raised to 500 °C at a ramp of 10 °C·min^{-1} and the signal of CO_2 (m/z = 44) and CO (m/z = 28) were recorded. CO chemisorption was carried out on the same instrument at 35 °C after H_2 treatment at 500 °C.

H_2 temperature-programmed reduction (H_2-TPR) measurements for the catalysts samples were conducted on Micromeritics Autochem II 2920 instrument equipped with a TCD detector. After pre-treatment in the flow of air in a quartz U-tube reactor at 500 °C for 60 min, the samples were cooled to ambient temperature in Ar flow. Then, 10% H_2/Ar flow was introduced to pass through the catalyst bed until a stable TCD signal was observed. Subsequently, a temperature ramping program from ambient to 1000 °C at the rate of 10 °C·min^{-1} was performed; H_2 consumption was monitored by TCD after removal of H_2O.

In situ diffuse reflectance infrared Fourier Transform spectroscopy (DRIFTS) experiments were performed on an FTIR spectrometer (Nicolet is-50) equipped with a smart collector and an MCT/A detector cooled by liquid nitrogen. The reaction temperature was controlled by

UNCORRECTED PROOF

an Omega programmable temperature controller (±1 °C). Prior to each experiment, the sample was pre-treated at 500 °C for 60 min in H_2 and then cooled to 300 °C. The background spectra were collected in flowing Ar and automatically subtracted from the sample spectrum. The reaction conditions were controlled as follows: 5% H_2, 20% CO_2 and Ar balance with total flow rate of 200 mL·min^{-1} (25 °C, 1 atm). All spectra were recorded by accumulating 100 scans with a resolution of 4 cm^{-1}.

3. Results and discussion

3.1. Catalytic performance of Ni/Y_2O_3-HN catalysts

The CO_2 hydrogenation reaction was performed on Ni/Y_2O_3-HN catalysts with various Ni loadings and performance of different catalysts is summarized in Fig. 1. For all the tested catalysts, conversion and yield reached thermodynamic equilibrium at high temperatures within the range tested. With the increase in Ni loading, catalytic activity increased, evidenced by the shift of the CO_2 conversion patterns to lower temperatures. In the case of the 2% Ni/Y_2O_3 catalyst, CO_2 conversion increased monotonically with the increase in temperature, reaching a value of 78% at 425 °C that was close to equilibrium. It is worth mentioning that activity of the 10% and the 20% Ni/Y_2O_3 catalysts reached equilibrium limitation (88%) at a temperature as low as 350 °C. However, doubling Ni loading from 10% to 20% only resulted in an unappreciable increase of about 4% in the CO_2 conversion at temperatures between 275 to 325 °C. On the other hand, the maximum yield of CO was below 4% for all the Ni/Y_2O_3-HN catalysts tested (Fig. 1B).

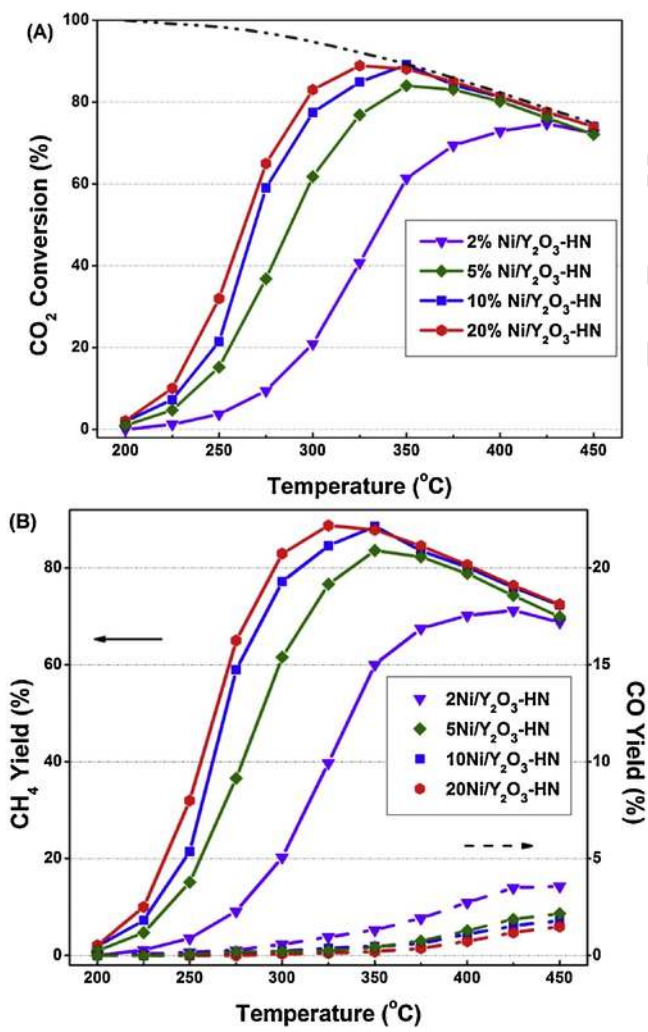

Fig. 1. (A) CO_2 conversion and (B) yields of CH_4 and CO over Ni/Y_2O_3-HN catalysts with different Ni loadings. Dashed line is the thermodynamic equilibrium conversion values.

3.2. Resistance to CO poisoning of the Ni/Y_2O_3-HN catalysts

Deactivation of Ni active sites caused by CO poisoning is a serious issue that cannot be ignored in practical application of Ni catalysts in CO_2 methanation. Introduction of CO leads to formation of $Ni(CO)_4$ species and their high mobility results in sintering of metal particles and, hence, poor catalysts long-term stability. To study stability of catalysts to CO poisoning, the reaction was performed with 1% CO in the feed over three Ni/Y_2O_3-HN catalysts with different Ni loadings.

As shown in Fig. 2, no evident loss of activity was observed in the case of the 5% Ni/Y_2O_3-HN catalyst within 80 h on stream. A slight decline in activity, with CO_2 conversion declining from 60% to 54% and 55% to 52% was observed in the cases of the 10% and the 20% Ni/Y_2O_3-HN catalysts, respectively. In contrast, no change in activity was observed in the CO-free experiments at the same temperature. The initial CO_2 conversion decreased by *ca.* 4% right after the addition of CO, which was caused by competitive adsorption of CO and CO_2 [30]. This result suggested that deactivation was caused by CO-poisoning rather than the heat-induced metal sintering, which was possibly affected by the interaction of Ni sites with Y_2O_3 support. This relation will be discussed below.

3.3. Characterization of the Ni/Y_2O_3-HN catalysts

$Y_4O(OH)_9(NO_3)$ as a Y-based support precursor affords a unique matrix to allow interactions with Ni^{2+} ions to form the Ni/Y_2O_3-HN catalysts. The precursor with impregnated Ni species evolves into the Y_2O_3-supported Ni nanoparticles in the process of calcination. Reflections of $Y_4O(OH)_9(NO_3)$ precursor were clearly identified by PXRD pattern, as shown in Fig. 3A. Distinct diffraction peaks assigned to Y_2O_3 were observed in the PXRD patterns of the Ni/Y_2O_3-HN catalysts with different Ni loadings, indicating phase transformation of the Y-based support from hydroxide hydrate to oxide (Fig. 3B). However, no Ni- or NiO-related diffraction peaks emerged over the Ni/Y_2O_3-HN catalysts with low Ni loadings (2 to 10%), suggested that Ni sites were either highly dispersed on Y_2O_3 surface, or existed in amorphous form in the as-prepared catalysts. The peaks at 37.2° and 62.8° became distinguishable when Ni loading was increased to 20 wt%, indicating formation of NiO phase.

CO_2-TPD was carried out to examine the surface basicity of the Ni/Y_2O_3-HN catalysts and their interactions with CO_2. As shown in Fig. 4, only one peak at around 82 °C was observed over the 2% Ni/Y_2O_3-HN catalyst; this peak was attributed to desorption of CO_2 adsorbed on weak basic sites. With the increase in Ni loading to 5%, the CO_2 desorption from weak basic sites was increased, while a small peak at *ca.* 240 °C appeared, which was indicative of desorption of CO_2 from the medium-strength basic sites. A further increase in the Ni content to 10% did not influence CO_2 desorption from the weak basic sites but led to the increase in the desorption volume of CO_2 from the medium-strength basic sites. An extra peak at a higher temperature of *ca.* 318 °C was observed when Ni content was changed to 20%, indicating the presence of an appreciable amount of strong basic sites.

It was suggested that CO_2 adsorbed on surface hydroxyls with weak basicity is effectively converted to active carbonate species, which further react with the dissociated H atoms to form CH_4 [31]. In addition, combining CO_2-TPD with DRIFTS studies, Pan et al. reported that surface oxygen sites with medium basicity promote formation of active monodentate carbonates and the subsequent transformation into CH_4,

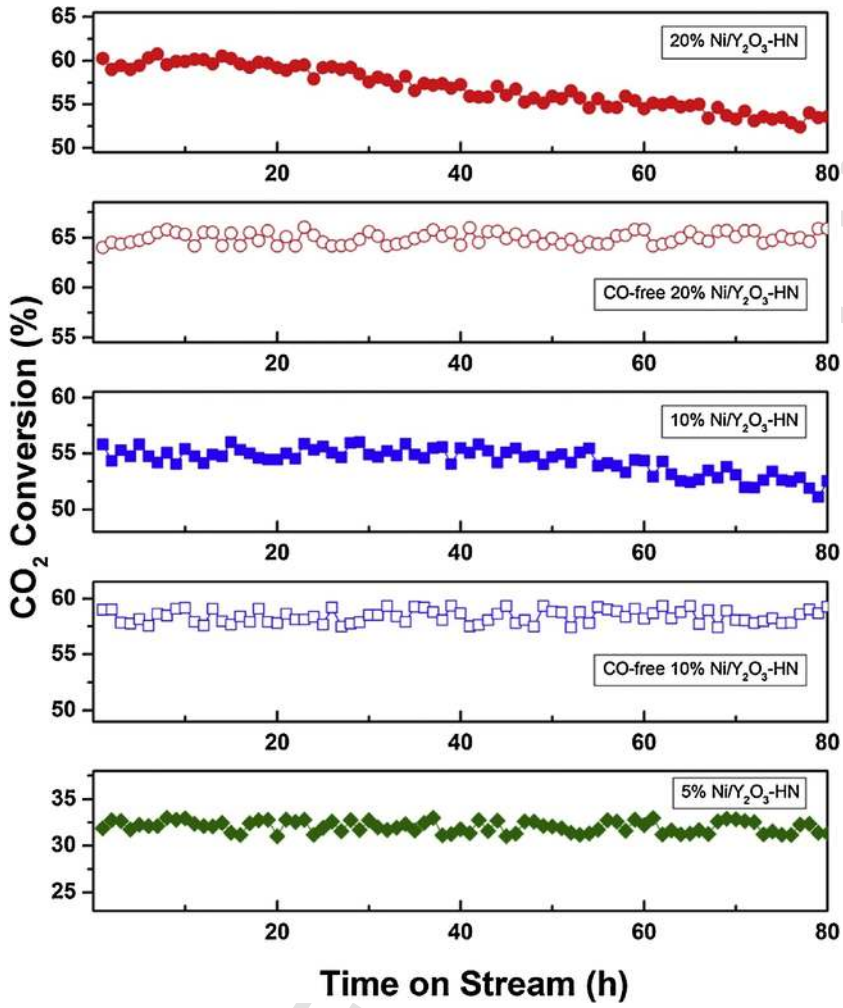

Fig. 2. Anti-CO-poisoning stability tests of Ni/Y_2O_3-HN catalysed CO_2 methanation reaction, which were run at 275 °C.

whereas CO_2 adsorbed on strong basic sites is not involved in the methanation reaction [32–34]. This offers an explanation why the 5% and the 10% Ni/Y_2O_3-HN catalysts with moderate basicity show good catalytic activity. It also agrees well with the fact that only minor increase in activity was observed when Ni loadings double from 10% to 20%.

To investigate the cause of deactivation, TG and H_2-TPR analysis were performed on the spent Ni-Y_2O_3 catalysts after long-term CO-fed CO_2 hydrogenation reaction. TG curves revealed no distinguishable weight loss during temperature ramp up to 800 °C for both the fresh and the spent 10% Ni/Y_2O_3-HN catalysts, indicating that there was no obvious carbon deposition during the reaction. Therefore, the possibility of deactivation caused by carbon deposition can be convincingly excluded. On the other hand, there was a noticeable difference in the H_2-TPR curves for the fresh and the spent catalysts, as shown in Fig. 5. Only one prominent peak at 325 °C was observed over the fresh 10% Ni/Y_2O_3-HN and the 20% Ni/Y_2O_3-HN, which was assigned to the Ni species weekly interacting with the Y_2O_3 support [29,35]. After 80 h of the CO-containing CO_2 reduction reaction, a small shoulder peak at 290 °C was observed for both samples, which was attributed to the reduction peak of the unsupported Ni species of lower activity for CO_2 methanation [8,36]. The appearance of this new peak confirmed the transformation of active Ni species into mobile Ni, which was caused by gradual poisoning by CO.

3.4. Effects of Y-precursors

3.4.1. Y-precursors determine catalyst structure

The metal-support interaction can be regulated by a choice of the suitable support material as well as by incorporating promoters, thus modulating catalytic activity and stability to CO poisoning [36]. However, the activity-structure-relationship is hard to reveal because several aspects of structural information are varied simultaneously. One effective strategy is to use several precursors of the same support to minimize the variations in structural parameters. For instance, by varying precursors of Al-support, the density of surface hydroxyl groups can be adjusted to anchor the Ag^+ species. As the metal-oxide interaction was successfully tuned, the as-prepared Ag/Al_2O_3 catalysts displayed good catalytic activity for selective reduction of NO_x [37]. We expect to control the strength of metal-support interaction by varying pre-calcination conditions of the Y-based support precursors and then to further optimize the catalytic activity of Ni/Y_2O_3 catalysts.

We shown that $Y_4O(OH)_9(NO_3)$ precursor was a unique support matrix for interaction with Ni species. Calcination of $Y_4O(OH)_9(NO_3)$ leads to the evolution of the Y_2O_3 phase, which proceeds *via* an intermediary phase, $YO(NO_3)$ (oxide nitrate: ON). This is evidenced from results of the combined TG and PXRD analysis. Three stages of weight loss were observed in the TG curve of $Y_4O(OH)_9(NO_3)$ precursor, as shown in Fig. 6. Based on the PXRD patterns for the products calcined at different temperatures, the weight loss before 300 °C was due to desorption of

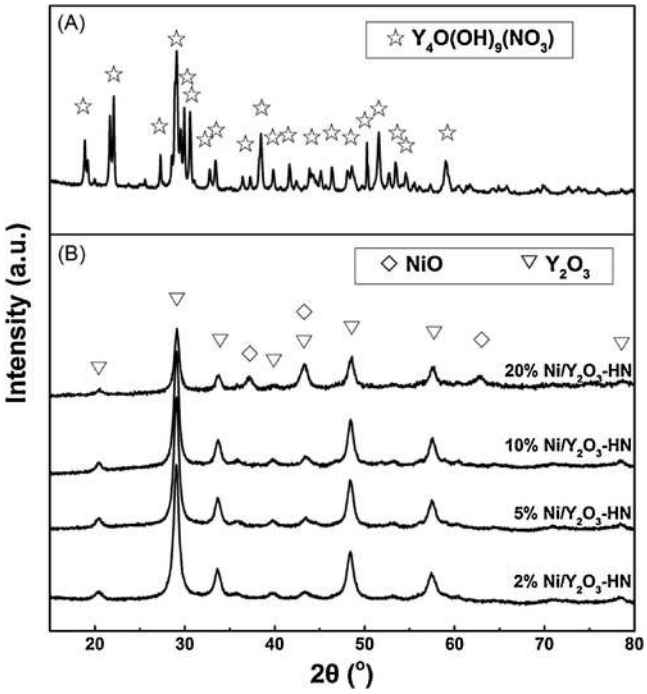

Fig. 3. PXRD patterns of (A) $Y_4O(OH)_9(NO_3)$ precursor and (B) Ni/Y_2O_3-HN catalysts with different Ni loadings.

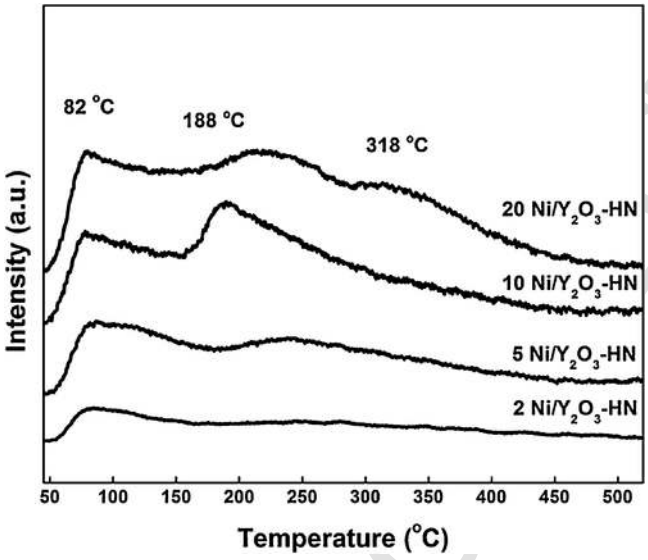

Fig. 4. CO_2-TPD profiles of Ni/Y_2O_3-HN catalysts with different Ni loadings.

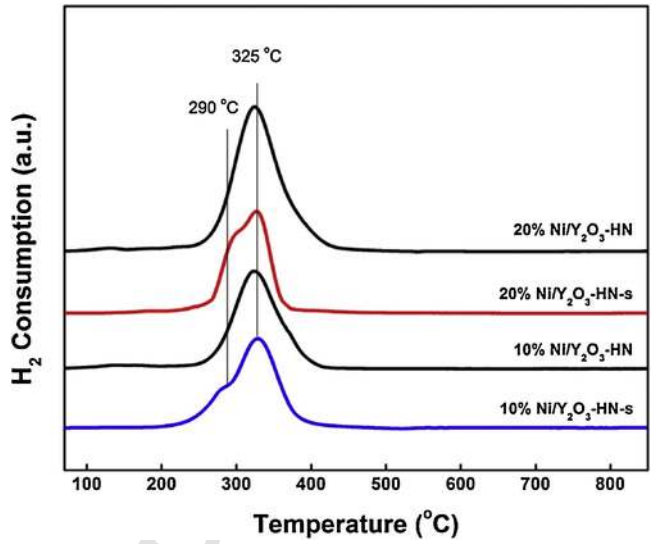

Fig. 5. H_2-TPR profiles of fresh 10% and 20% Ni/Y_2O_3-HN catalysts, along with the spent catalysts after CO poisoning test (denoted as Ni/Y_2O_3-HN-s).

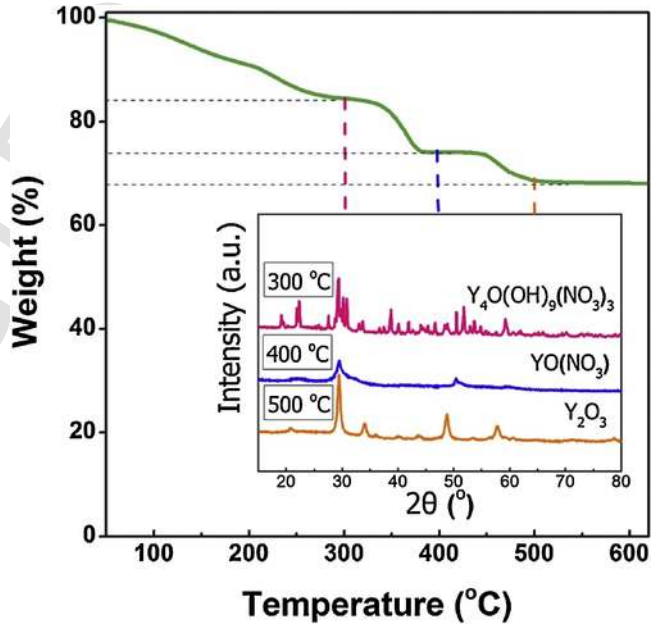

Fig. 6. TG profile of the products from hydrothermal treatment and the corresponding PXRD patterns of the calcined products at different temperature.

the physisorbed content and the phase of $Y_4O(OH)_9(NO_3)$ was still maintained at this temperature. The other two weight changes at approx. 400 and 500 °C were attributed to phase transitions, with the first one corresponding to the transition from $Y_4O(OH)_9(NO_3)$ (hydroxide nitrate: HN) to $YO(NO_3)$ and the second one from $YO(NO_3)$ to Y_2O_3 (oxide: OX).

To tune the metal-support interaction, the other two Y-precursors were prepared and used as supports in the synthesis of the 10% Ni/Y_2O_3 catalysts. Ni/Y_2O_3-HN, Ni/Y_2O_3-ON and Ni/Y_2O_3-OX were denoted according to their precursors, respectively. The PXRD patterns for the three as-prepared catalysts showed exclusive diffraction peaks of Y_2O_3 after calcination (Fig. S1). No Ni-related peaks appeared, as expected, indicating good dispersion of Ni species on the surface of Y_2O_3. Moreover, Ni content in the resulted catalysts, determined by ICP-EOS, was almost identical (Table 1). Uniform pore structures and BET surface areas were obtained, suggesting no evident structural variation between the catalysts has been introduced by varying the precursor.

The subtle distinctions in surface properties were observed on these three Ni/Y_2O_3 catalysts. The surface sites with both weak and medium basicity were reflected by CO_2-TPD curves of the three catalysts (Fig. S2). However, intensity and the amount of medium strength basic sites were different. The total CO_2 desorption peak area from the medium basic sites on the Ni/Y_2O_3-HN and the Ni/Y_2O_3-ON were similar, but significantly higher than that for the Ni/Y_2O_3-OX. The H_2-TPR profiles of the three Ni/Y_2O_3 catalysts revealed different types of H_2 reduction peaks, as shown in Fig. 7. Compared to the 10% Ni/Y_2O_3-HN catalyst, a shoulder peak at 351 °C appeared as well as the major peak at 325 °C, over the 10% Ni/Y_2O_3-ON catalyst. This was attributed to the strengthened metal-support interaction. For the 10% Ni/Y_2O_3-OX catalyst, the H_2-reduction peaks were drastically different. Intensity of the peak at

Table 1
BET surface area, average pore size and total pore volume estimated from the Brunauer-Emmett-Teller (BET) analysis, along with the Ni content determined by ICP-EOS, Ni dispersion from chemisorption and TOF of CO_2.

Sample	Surface area	Pore size	Pore volume	Ni content	Ni dispersion[a]	TOF[b]
	(m^2/g)	(nm)	(ml/g)	(%)	(%)	($\times10^{-3}$ s^{-1})
10% Ni/Y_2O_3-HN	77.14	3.14	0.19	10.11	18.6	8.55
10% Ni/Y_2O_3-ON	72.09	3.20	0.20	10.16	13.2	8.46
10% Ni/Y_2O_3-OX	74.66	3.08	0.19	10.05	9.7	7.13

[a] estimated from CO chemisorption by assuming the ratio of CO:Ni(surface) = 1:1.
[b] TOF of CO_2 at 225 °C (reacted CO_2 per surface Ni per second).

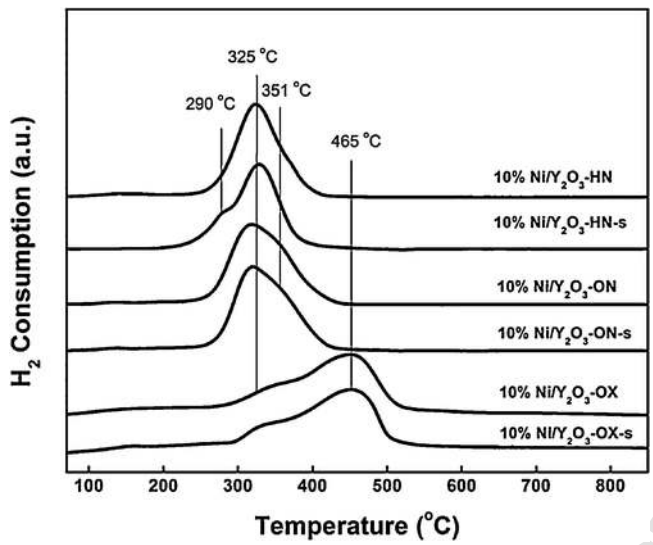

Fig. 7. H_2-TPR profiles of fresh and spent Ni/Y_2O_3 from different support precursors.

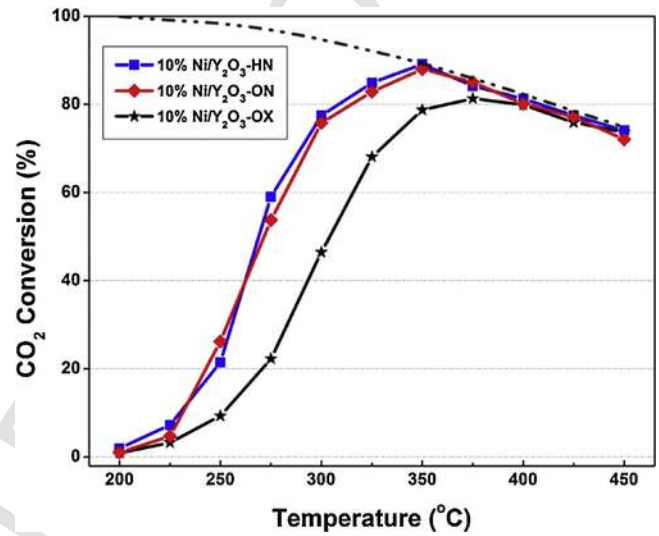

Fig. 8. CO_2 conversion over catalysts prepared from different support precursors. Dashed line is the thermodynamic equilibrium conversion values.

325 °C decreased and the major peak was at 465 °C that was assigned to the reduction of Ni species with a much stronger interaction with the support [37,38].

Based on the above analysis, we conclude that the nature of the Y-precursor could determine the surface basic properties and the interaction strength between Ni sites and Y_2O_3 supports while preserving the macrostructure of the support.

3.4.2. *Y-precursors determine stability to CO poisoning*

Catalytic reaction of CO_2 methanation was performed on the 10% Ni/Y_2O_3 catalysts derived from the three different Y-precursors. As shown in Fig. 8, the Ni/Y_2O_3-ON catalyst exhibited comparable CO_2 conversion to the Ni/Y_2O_3-HN catalyst, which reached 88% at 350 °C to track the equilibrium conversion. Similar distributions of surface sites with medium basicity were one of the primary causes of high activity of these two catalysts. The Ni/Y_2O_3-OX catalyst showed relatively lower activity, which was reflected in the conversion curve being shifted to higher temperatures. One reason of the lower CO_2 conversion over the Ni/Y_2O_3-OX catalyst was the weak surface interaction with CO_2, as evidenced by the reduction in the amount of the medium strength basic sites in the CO_2-TPD profile.

It has been generally accepted that metallic Ni served as the active sites for H_2 dissociation and CO_2 methanation [11,39]. However, using *in situ* EXAFS characterization, Du and co-workers revealed that the mild oxidation atmosphere of CO_2 resulted in the partial oxidation of Ni^0 during methanation, which was closely related to reducibility of Ni species in the first place [40]. The oxidative status of Ni species also deteriorated the activity of CO_2 methanation. Therefore, although the catalysts were pre-treated in H_2 at 500 °C before activity tests, the Ni species in Ni/Y_2O_3-OX could be easily oxidized due to the strong NiO_x-Y_2O_3 interaction and this leds to inferior activity for CO_2 methanation.

We carried out CO chemisorption to determine the dispersion of Ni, assuming each exposed Ni site took up one CO molecule [39,41]. A considerably higher dispersion of Ni was observed over the Ni/Y_2O_3-HN, which was 18.6%. The dispersion of Ni in the Ni/Y_2O_3-ON and Ni/Y_2O_3-OX was 13.2% and 9.7%, respectively. This leads to a concern about variations in the size of Ni particles, which can affect catalytic performance as well as the reduction behavior [11,42]. To further investigate the effects of Ni particle size, HR-TEM analysis of the three Ni catalysts was performed. As shown in Fig. S3, Ni particles with an average diameter of 6.8, 7.0 and 7.3 nm for the pre-reduced Ni/Y_2O_3-HN, Ni/Y_2O_3-ON and Ni/Y_2O_3-OX catalysts, respectively, were observed. The similar particle size distributions but varied dispersions of Ni suggested that different shapes of metal particles have been adopted, which agreed well with the assumption of gradual emergence of Ni into the substance of the support due to the strengthened metal-support interaction. The TOF was calculated based on Ni dispersion. As shown in Table 1, a similar value was obtained over the Ni/Y_2O_3-HN and the Ni/Y_2O_3-ON, while an obvious decrease was observed over the Ni/Y_2O_3-OX. This suggests that an overly strong metal-support interaction deteriorated the methanation activity; this also agrees well with the possible consequence of Ni^0 oxidation over reaction time.

The stability to CO poisoning was further investigated over the three 10% Ni/Y_2O_3 catalysts (Fig. S4). Within 80 h on stream, a slight drop in conversion was observed in the case of the Ni/Y_2O_3-HN catalyst, assigned to the formation of mobile $Ni(CO)_4$ species (reduction peak at 290 °C in the H_2-TPR of the spent sample) as discussed previously. A low but constant CO_2 conversion, around 20%, was obtained in the case of the Ni/Y_2O_3-OX catalyst, while a stable conversion of

UNCORRECTED PROOF

around 53% was obtained in the case of the Ni/Y_2O_3-ON catalyst. The latter two spent samples were also examined by H_2-TPR (Fig. 7). The reduction peaks of strengthened $Ni\text{-}Y_2O_3$ interaction were unaffected and no peak of mobile Ni species on Y_2O_3 support at 290 °C was observed, suggesting that the strong interaction between Ni and Y_2O_3 hindered the formation of $Ni(CO)_4$ species. As shown in Fig. 9, the CO-TPD profiles evaluated the interaction between CO and the catalysts' surface, which revealed only one CO desorption peak at a temperature lower than 150 °C over the Ni/Y_2O_3-OX and the Ni/Y_2O_3-ON, owing to the physically adsorbed CO species. For the Ni/Y_2O_3-HN, another prominent peak at a higher temperature of ~350 °C appeared, which originated from desorption of CO that strongly interacted with Ni species. This result clearly suggested that the metal-support interaction affected the affinity of CO to the surface, determining stability of Ni catalysts in CO-containing reaction mixtures.

A fine-tuning of the interaction between Ni and the Y_2O_3 supports is required to realize simultaneously superior methanation activity and robust stability. Pretreatment by H_2 at 500 °C successfully reduces NiO into active metallic Ni species, which is stabilized by surface anchoring sites. On the one hand, a metal-support interaction that is too weak results in vulnerability to sintering of Ni particles over long-term catalytic runs, especially when CO is introduced. On the other hand, if the interaction between Ni species and the support is too strong, the surface Ni species cannot retain the active metallic state in the reaction atmosphere, which results in the deteriorated catalytic performance [43,44]. Ideally, the metal-support interaction should be strong enough to offer sufficient anchoring sites for the highly dispersed active sites, but not too strong to prevent the Ni species from being maintained in the active metallic form. Choosing a suitable Y-precursor can afford a moderate interaction between the Ni species and Y_2O_3 support, which is beneficial to the enhancement in catalytic activity and stability.

The catalytic activity and anti-CO-poisoning ability for Y_2O_3 supported Ni catalysts are affected by the degree of dispersion of Ni species and the strength of metal-support interaction. In Ni/Y_2O_3-HN, a high dispersion of Ni has been obtained. However, the weak metal-support interaction offered few anchoring sites for the active sites, which were vulnerable to CO poisoning. As a comparison, a much stronger metal-support interaction has been achieved over the Ni/Y_2O_3-OX, which benefited the anchoring of active Ni species, thus improved the stability in CO-containing reaction gas. However, this also led to the decrease in the number of active sites exposed on the surface as most of Ni atoms were within the matrix of the support. In addition, the high reduction temperature of Ni species with a strong metal-support interaction resulted in the partial oxidation of the metallic Ni in the mild oxidative atmosphere of methanation reaction, which further decreased the available active sites [40]. In between, the structure of $YO(NO_3)$ provided a moderate metal-support interaction, which was strong enough to prevent the formation of mobile Ni carbonyls in CO atmosphere at almost no expense on the exposed Ni sites. Thus, simultaneously improved stability and excellent activity have been achieved over Ni/Y_2O_3-ON.

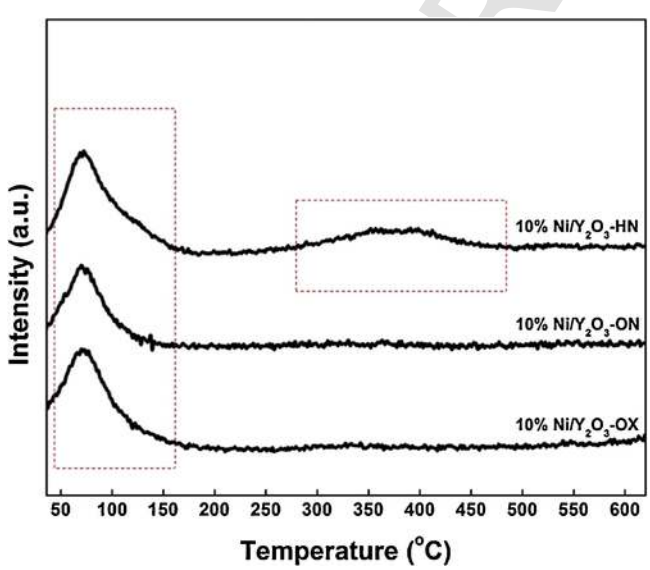

Fig. 9. CO-TPD profiles of Ni/Y_2O_3 prepared from different support precursors.

3.5. Surface reaction intermediates and mechanisms

In consideration of distinct surface basicity and $Ni\text{-}Y_2O_3$ interaction for the Ni/Y_2O_3-HN and the Ni/Y_2O_3-OX catalysts, the surface intermediates and the reaction pathways on the two catalysts may potentially differ during the CO_2 methanation process. *In situ* DRIFTS experiments were performed to study the evolution of surface species during CO_2 hydrogenation. The spectra were recorded after adsorption of CO_2 for 30 min at 300 °C over the 10% Ni/Y_2O_3-HN with He purge for 60 min to remove the physisorbed CO_2 and any gaseous residues. After that the inlet gas was switched to H_2 while evolution of the surface species was monitored.

As shown in Fig. 10, adsorption of CO_2 resulted in the formation of two bands centered at 1512 and 1378 cm^{-1}, along with a distinct band at 1296 cm^{-1}, all of which were attributed to different carbonates species [10,45,46]. Moreover, shoulder peaks at 1655, 1592, 1443 and 1211 cm^{-1} were clearly distinguishable. While the band at 1592 cm^{-1} was also ascribed to surface carbonates species, the other three peaks were assigned to hydrogen carbonates [29,47–49]. The introduction of H_2 resulted in the immediate appearance of new bands at 1621, 1601, 1362 and 1341 cm^{-1}, accompanied by apparent attenuation of the carbonates bands at 1592, 1512, 1378, and 1296 cm^{-1}. The four new peaks were divided into two groups: (*i*) 1621 and 1341 cm^{-1}, and (*ii*) 1601 and 1362 cm^{-1}, which were assigned to monodentate formate species and bidentate formate species, respectively, on the basis of the frequency difference between the two peaks [33,50,51]. Most importantly, the peaks at 3010 and 1301 cm^{-1}, which were assigned to methane, appeared after the introduction of H_2 (Fig. 10A). The bands of formate species reached a maximum in 5 min with the continuous consumption of carbonates, suggesting a transformation of carbonates into formate species with the steady supply of H_2, which agreed well with the literature [52,53]. After that, the peaks of formate species decreased, along with the continuous formation of surface methane species. According to the obtained DRIFTS spectra, we conclude that the possible complete reaction route of the CO_2 methanation catalyzed by the Ni/Y_2O_3 proceeds with formation of carbonates following adsorption of CO_2, which are first hydrogenated into formate and subsequently transformed into methane as the final product.

A different evolution route of surface intermediates was evident from the DRIFTS results obtain with the 10% Ni/Y_2O_3-OX catalyst. As shown in Fig. 10D, a similar spectrum at the stage of CO_2 adsorption was obtained, which revealed the peaks of carbonates at 1592, 1512, 1378 and 1296 cm^{-1}, along with hydrogen carbonates at 1655, 1443 and 1211 cm^{-1}. Moreover, the monodentate formate peaks at 1621 and 1341 cm^{-1} were recognizable, which probably was the result of CO_2 being adsorbed on the surface hydroxyl groups. After the introduction of H_2, hydrogen carbonates and carbonates species were generally consumed and appreciable amount of formate species were produced. However, unlike that on the 10% Ni/Y_2O_3-HN catalyst, the peaks ascribed to formate species were continuing to increase even after exposure to H_2 for 60 min. Noticeably, the peak at 3010 cm^{-1} of surface methane species diminished quickly and disappeared after 5 min, suggesting that conversion channel of formate spices into methane was closed. Based on the DRIFTS results, the reaction pathway on the 10%

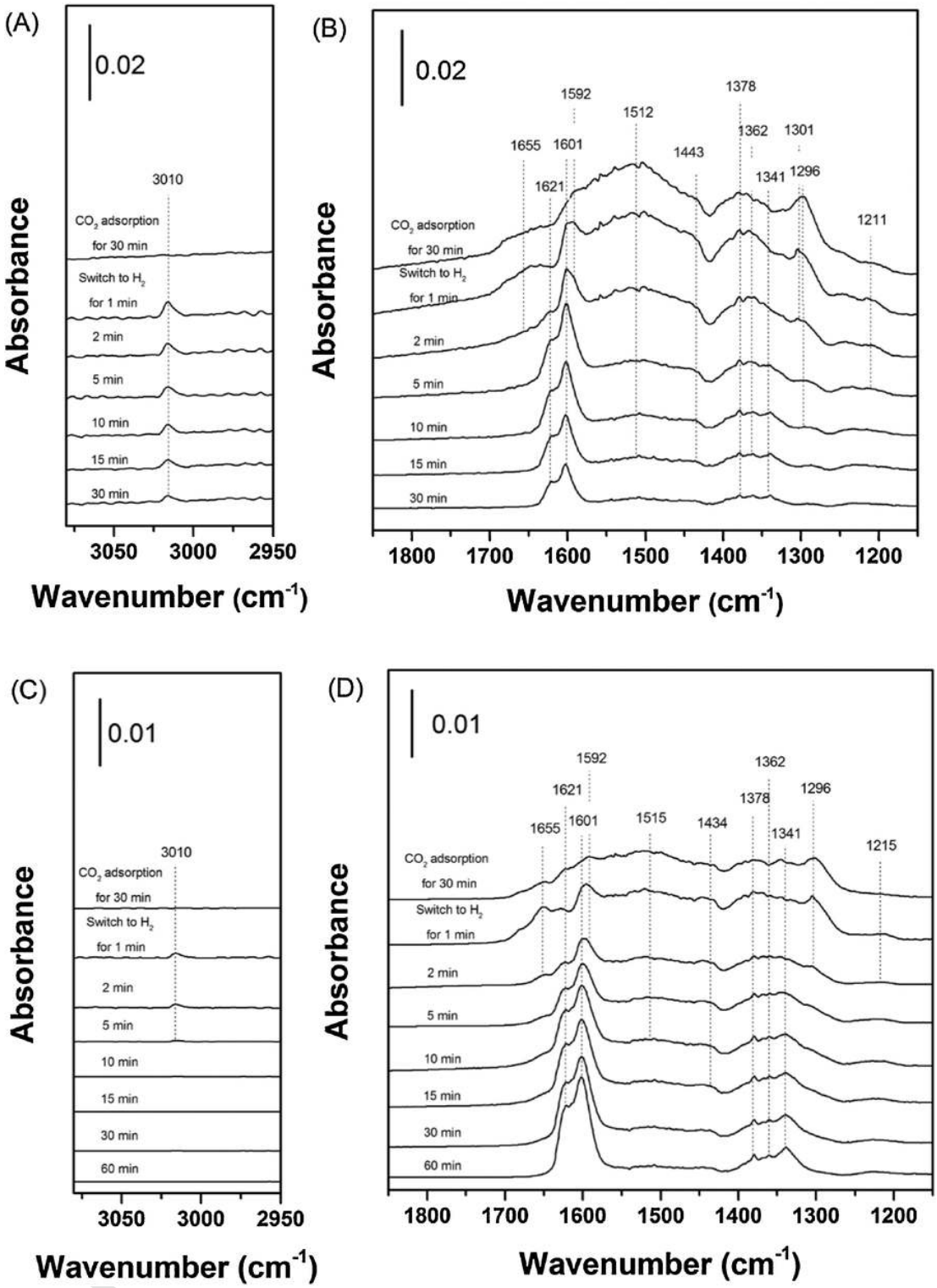

Fig. 10. Dynamic changes of *in situ* DRIFTS spectra over (A, B) 10% Ni/Y_2O_3 and (C, D) 10% $Ni\text{-}Y_2O_3$ recorded as a function of time in a flow of H_2 at 300 °C after being exposed to CO_2 for 30 min.

Ni/Y_2O_3-OX was proposed: the adsorbed CO_2 is first converted into formate specie and then formed into methane; the step of formate conversion has been significantly hindered over the 10% Ni/Y_2O_3-OX catalyst.

The reaction steps of CO_2 adsorption and carbonates formation occurred in a similar way on the two Ni/Y_2O_3 catalysts. However, after carbonates converted into formates, the following reaction pathways differed. A higher yield of methane was obtained on the Ni/Y_2O_3-HN catalyst due to sequential transformation of formates into methane. In the case of the Ni/Y_2O_3-OX catalyst, the rate of formation of the formate intermediate species was much higher than their rate of conversion into methane, possibly due to the lower rate of atomic H supply. This result is also in good agreement with the fact that conversion of formate species is the rate-determining step for CO_2 methanation [54]. The H_2 dissociation on metallic Ni sites significantly depends on the

dispersion. The lower dispersion of Ni over the Ni/Y_2O_3-OX led to a decrease in surface H concentration, which slowed the conversion of formate species and thus limited productivity of the Ni/Y_2O_3-OX catalyst towards methane.

4. Conclusions

Different Y-precursors were used to prepare Ni/Y_2O_3 catalysts to tune the metal-support interaction without affecting morphology of the catalysts. Catalysts prepared starting from $YO(NO_3)$ precursor resulted in a moderate metal-support interaction, showing superior activity for CO_2 methanation and robust stability in CO-containing reaction mixtures. A weak metal-support interaction caused poorer stability over catalysts prepared from $Y_4O(OH)_9(NO_3)$, while inferior activity was obtained when Y_2O_3 was used, which was the result of an overly strong metal-support interaction. Spectroscopic study by DRIFTS showed that carbonates were formed after CO_2 adsorption, which were then converted into formates and methane stepwise after the introduction of H_2, the latter step being affected in the case of the catalyst with a strong metal-support interaction.

Acknowledgments

This project was funded by the National Research Foundation (NRF), Prime Minister's Office, Singapore under its Campus for Research Excellence and Technological Enterprise (CREATE) program.

Appendix A. Supplementary data

Supplementary material related to this article can be found, in the online version, at doi:https://doi.org/10.1016/j.apcatb.2018.06.021.

References

[1] National Oceanic & Atmospheric Administration, USA, The NOAA Annual Greenhouse Gas Index (AGGI), 2017 http://www.esrl.noaa.gov/gmd/aggi/aggi.html.
[2] A. Kudo, Y. Miseki, Chem. Soc. Rev. 38 (2009) 253.
[3] S.P. Wang, S.L. Yan, X.B. Ma, J.L. Gong, Energy Environ. Sci. 4 (2011) 3805.
[4] A. Goeppert, M. Czaun, G.K.S. Prakash, G.A. Olah, Energy Environ. Sci. 5 (2012) 7833.
[5] M. Peters, B. Kohler, W. Kuckshinrichs, W. Leitner, P. Markewitz, T.E. Muller, ChemSusChem 4 (2011) 1216.
[6] L. Falbo, M. Martinelli, C.G. Visconti, L. Lietti, C. Bassano, P. Deiana, Appl. Catal. B: Environ. 225 (2018) 354.
[7] I. Graça, L.V. González, M.C. Bacariza, A. Fernandes, C. Henriques, J.M. Lopes, M.F. Ribeiro, Appl. Catal. B: Environ. 147 (2014) 101.
[8] J. Liu, J. Yu, F. Su, G. Xu, Catal. Sci. Tech. 4 (2014) 472.
[9] M.-C. Silaghi, A. Comas-Vives, C. Copéret, ACS Catal. 6 (2016) 4501.
[10] M. Tao, X. Meng, Z. Xin, Z. Bian, Y. Lv, J. Gu, Appl. Catal. A: Gen. 516 (2016) 127.
[11] C. Vogt, E. Groeneveld, G. Kamsma, M. Nachtegaal, L. Lu, C.J. Kiely, P.H. Berben, F. Meirer, B.M. Weckhuysen, Nat. Catal. 1 (2018) 127.
[12] J. Gao, Y. Wang, Y. Ping, D. Hu, G. Xu, F. Gu, F. Su, RSC Adv. 2 (2012) 2358.
[13] H. Liu, X. Zou, X. Wang, X. Lu, W. Ding, J. Nat. Gas Chem. 21 (2012) 703.
[14] M. Agnelli, M. Kolb, C. Mirodatos, J. Catal. 148 (1994) 9.
[15] W.M. Shen, J.A. Dumesic, C.G. Hill Jr, J. Catal. 68 (1981) 152.
[16] C. Mirodatos, H. Praliaud, M. Primet, J. Catal. 107 (1987) 275.
[17] M. Tan, X. Wang, X. Wang, X. Zou, W. Ding, X. Lu, J. Catal. 329 (2015) 151.
[18] H. Liu, H. Wu, D. He, Fuel Process. Technol. 119 (2014) 81.
[19] Y. Wang, R. Wu, Y. Zhao, Catal. Today 158 (2010) 470.
[20] W. Li, X. Nie, X. Jiang, A. Zhang, F. Ding, M. Liu, Z. Liu, X. Guo, C. Song, Appl. Catal. B: Environ. 220 (2018) 397.
[21] W. Xia, F. Wang, X. Mu, K. Chen, A. Takahashi, I. Nakamura, T. Fujitani, Catal. Commun. 90 (2017) 10.
[22] P. Gao, L. Zhong, L. Zhang, H. Wang, N. Zhao, W. Wei, Y. Sun, Catal. Sci. Tech. 5 (2015) 4365.
[23] Y. Cao, X. Feng, H. Xu, L. Lan, M. Gong, Y. Chen, Catal. Commun. 76 (2016) 33.
[24] L. Sun, Y. Tan, Q. Zhang, H. Xie, F. Song, Y. Han, Int. J. Hydrogen Energy 38 (2013) 1892.
[25] G.B. Sun, K. Hidajat, X.S. Wu, S. Kawi, Appl. Catal. B: Environ. 81 (2008) 303.
[26] J. Sun, X.-P. Qiu, F. Wu, W.-T. Zhu, Int. J. Hydrogen Energy 30 (2005) 437.
[27] U. Oemar, K. Hidajat, S. Kawi, Int. J. Hydrogen Energy 40 (2015) 12227.
[28] H.W. Wijaya, T. Kojima, T. Hara, N. Ichikuni, S. Shimazu, ChemCatChem 9 (2017) 2869.
[29] H. Muroyama, Y. Tsuda, T. Asakoshi, H. Masitah, T. Okanishi, T. Matsui, K. Eguchi, J. Catal. 343 (2016) 178.
[30] B. Nematollahi, M. Rezaei, E.N. Lay, Int. J. Hydrogen Energy 40 (2015) 8539.
[31] P.A.U. Aldana, F. Ocampo, K. Kobl, B. Louis, F. Thibault-Starzyk, M. Daturi, P. Bazin, S. Thomas, A.C. Roger, Catal. Today 215 (2013) 201.
[32] L. He, Q. Lin, Y. Liu, Y. Huang, J. Energ. Chem. 23 (2014) 587.
[33] Q.S. Pan, J.X. Peng, T.J. Sun, S. Wang, S.D. Wang, Catal. Commun. 45 (2014) 74.
[34] J. Huang, Y. Wang, J. Zheng, W.-L. Dai, K. Fan, Appl. Catal. B: Environ. 103 (2011) 343.
[35] H. Liu, D. He, Int. J. Hydrogen Energy 36 (2011) 14447.
[36] Y. Yan, Y. Dai, H. He, Y. Yu, Y. Yang, Appl. Catal. B: Environ. 196 (2016) 108.
[37] R.D. Zhang, S. Kaliaguine, Appl. Catal. B: Environ. 78 (2008) 275.
[38] Y.B. Yu, J.J. Zhao, Y. Yan, X. Han, H. He, Appl. Catal. B: Environ. 136 (2013) 103.
[39] L.R. Winter, E. Gomez, B. Yan, S. Yao, J.G. Chen, Appl. Catal. B: Environ. 224 (2018) 442.
[40] G.A. Du, S. Lim, Y.H. Yang, C. Wang, L. Pfefferle, G.L. Haller, J. Catal. 249 (2007) 370.
[41] M. Kiskinova, D.W. Goodman, Surf. Sci. 108 (1981) 64.
[42] A. Parmaliana, F. Arena, F. Frusteri, N. Giordano, J. Chem. Soc., Faraday Trans. 86 (1990) 2663.
[43] M.A.A. Aziz, A.A. Jalil, S. Triwahyono, R.R. Mukti, Y.H. Taufiq-Yap, M.R. Sazegar, Appl. Catal. B: Environ. 147 (2014) 359.
[44] M.A.A. Aziz, A.A. Jalil, S. Triwahyono, S.M. Sidik, Appl. Catal. A: Gen. 486 (2014) 115.
[45] Y.X. Pan, C.J. Liu, Q.F. Ge, J. Catal. 272 (2010) 227.
[46] P. Panagiotopoulou, D.I. Kondarides, X.E. Verykios, J. Phys. Chem. C 115 (2011) 1220.
[47] F.Z. Zhao, Z.Y. Liu, W.Q. Xu, S.Y. Yao, A. Kubacka, A.C. Johnston-Peck, S.D. Senanayake, A.Q. Zhang, E.A. Stach, M. Fernandez-Garcia, J.A. Rodriguez, J. Phys. Chem. C 118 (2014) 2528.
[48] S. Fujita, M. Nakamura, T. Doi, N. Takezawa, Appl. Catal. A: Gen. 104 (1993) 87.
[49] G. Garbarino, P. Riani, L. Magistri, G. Busca, Int. J. Hydrogen Energy 39 (2014) 11557.
[50] H.C. Wu, Y.C. Chang, J.H. Wu, J.H. Lin, I.K. Lin, C.S. Chen, Catal. Sci. Tech. 5 (2015) 4154.
[51] A. Westermann, B. Azambre, M.C. Bacariza, I. Graça, M.F. Ribeiro, J.M. Lopes, C. Henriques, Appl. Catal. B: Environ. 174–175 (2015) 120.
[52] M. Marwood, R. Doepper, A. Renken, Appl. Catal. A: Gen. 151 (1997) 223.
[53] S. Tada, O.J. Ochieng, R. Kikuchi, T. Haneda, H. Kameyama, Int. J. Hydrogen Energy 39 (2014) 10090.
[54] F. Wang, S. He, H. Chen, B. Wang, L. Zheng, M. Wei, D.G. Evans, X. Duan, J. Am. Chem. Soc. 138 (2016) 6298.

UNCORRECTED PROOF